Environmental Pollution 295 (2022) 118697

Contents lists available at ScienceDirect

Environmental Pollution

journal homepage: www.elsevier.com/locate/envpol

Temporal evolution of acid mine drainage (AMD) leachates from the abandoned tharsis mine (Iberian Pyrite Belt, Spain)☆

Raúl Moreno-González, Francisco Macías, Manuel Olías, Carlos Ruiz Cánovas *

Department of Earth Sciences & Research Center on Natural Resources, Health and the Environment. University of Huelva, Campus "El Carmen", E-21071, Huelva, Spain

ARTICLE INFO

Highlights:
Metal transport
High-resolution sampling
Mining wastes
Chronic pollution
Remediation measures

ABSTRACT

Acid mine drainage (AMD) due to the mining of sulfide deposits is one of the most important causes of water pollution worldwide. Remediation measures, especially in historical abandoned mines, require a deep knowledge of the geochemical characteristics of AMD effluents and metal fluxes, considering their high spatial and temporal evolution, and the existence of point and diffuse sources with a different response to rainfall events. This study investigates the temporal variations and hydrogeochemical processes affecting the composition of main AMD sources from the Tharsis mines (SW Spain), one of most important historical metal mining districts in the world. To address this, a fortnightly-monthly sampling was performed during two years in the main AMD sources and streams within the mine site covering different hydrological conditions. A seasonal pattern was observed linked to hydrological variations; higher pollutant concentrations were observed during the dry season (maximum values of 4,6 g/L of Al, 11,8 g/L of Fe, and 67 g/L of sulfate) and lower ones were observed during the rainy periods. Stream samples exhibited a negative correlation between electrical conductivity (EC) and flow, while positive values were observed in AMD sources, where groundwater fluxes were predominant. High flow also seems to be the main driver of Pb fluxes from AMD sources, as the concentration of Pb in waters increased notably during these events. The precipitation of secondary Fe minerals may limit the mobility of As and V, being retained in the proximity of mine sites. The concentration of Zn in waters seems to be controlled by the original grade in the metal deposit from which the waste is generated, together with the age of these wastes. The pollutant load delivered by the Tharsis mines to the surrounding water courses is very high; e.g., mean of 733 ton/yr of Al or 2757 ton/yr of Fe, deteriorating the streams and reservoirs downstream.

1. Introduction

Acid mine drainage (AMD) from sulfide and carbon deposits is one of the main environmental problems affecting water resources (Akcil and Koldas, 2006). Sulfides are stable minerals upon anoxic conditions; however, when exposed to oxygen and water, these minerals are oxidized leading to the formation of AMD. This process may also happen naturally when these minerals outcrop at the Earth's surface (in this case the process is called acid rock drainage -ARD-; Nordstrom et al., 2015). However, mining activities may boost the generation of acid waters by increasing the volume of sulfides exposed. Thus, AMD is considered one of the main factors responsible for water quality degradation worldwide, including ground and surface waters. For example, around 19,300 km of rivers and 720 km^2 of lakes and reservoirs throughout the world were severely affected by AMD at the end of the last century (Johnson and Hallberg, 2005). This environmental concern is especially relevant in areas suffering from historical metal mining activities, where the application of less efficient mineral extraction and processing techniques, and the lack of environmental awareness and controls have left huge environmental liabilities (Bird, 2016). This is the case of the Iberian Pyrite Belt (IPB), where approximately 150 years of modern mining has resulted in the generation of enormous volumes of metal-rich wastes; approximately 48 km^2 of the surface is occupied by waste rock piles, open pits, tailing dams, and other mining facilities only in the Spanish sector (Grande et al., 2014). The oxidation of sulfides contained in these wastes has caused the chronic pollution of the main watersheds in the IPB, the Odiel and Tinto rivers, which can be considered as extreme examples of AMD pollution worldwide (Cánovas et al., 2021).

☆ This paper has been recommended for acceptance by Dr. Jörg Rinklebe.

* Corresponding author.
E-mail address: carlos.ruiz@dgeo.uhu.es (C. Ruiz Cánovas).

https://doi.org/10.1016/j.envpol.2021.118697
Received 1 September 2021; Received in revised form 4 December 2021; Accepted 14 December 2021
Available online 17 December 2021

Among the tens of old mines within the IPB, Tharsis is the second in importance after the well-known Rio Tinto mines (Moreno-González et al., 2020). Intense mining activities have left a huge environmental legacy, with a total surface affected by mining of around 4,13 km^2, including soils, waste heaps, and pit lakes. Intense sulfide oxidation processes in this area have caused a general deterioration of the surrounding water quality (Masbou et al., 2020; Moreno-González et al., 2020), especially in the Sancho Reservoir (capacity of 58 hm^3), located downstream of the mining area and fed by the acidic Meca River, which exhibits pH values close to 3.5 and high concentrations of trace metals (Cánovas et al., 2016a). This acidification might happen again in the Alcolea reservoir (246 hm^3), which is currently under construction. The high load of pollutants delivered by different mines placed in the reservoir drainage basin (Tharsis among them) has put in doubt the final quality of the stored waters (Olías et al., 2011) and evidences the urgent need for the implementation of remediation measures in these mine sites. On the other hand, remediation actions to limit the environmental impact of abandoned metal mines are strongly demanded by the EU Water Framework Directive (EU Commission, 2000). However, these remediation measures require a deep knowledge of the geochemical characteristics of AMD effluents, considering their high spatial and temporal evolution, as well as the existence of point and diffuse sources with different responses to rainfall.

In this sense, there is a general lack of detailed information on AMD sources based on time datasets collected in synoptic samplings, and only a few examples can be found in literature (e.g., Mighanetara et al., 2009; Cánovas et al., 2018; Vriens et al., 2019). Therefore, the main aims of this work are: i) to study the temporal variations of main AMD sources and streams of the Tharsis mines; and ii) to clarify the geochemical processes (e.g., mineral precipitation/dissolution) affecting the hydrochemical composition of these different AMD sources (i.e., diffuse and point sources).

2. Study area

The Tharsis Mine Complex (Fig. 1) consists of different sulfide mines located in southwestern Spain, which have been exploited since antiquity by Tartessians and Romans (Gonzalo y Tarín, 1888; Pinedo Vara, 1963). Most metal extraction occurred from 1856 to 2001 when around 40 Mt of sulfide was obtained with an average ore grade of 1.8% of Zn, 0.8% of Pb, and 0.7% of Cu (Leistel et al., 1998; Tornos et al., 1998, Tornos, 2006; 2009). Although mining activities in Tharsis ceased in 2001, the reopening of the mine is currently being considered. The study area exhibits a high level of AMD pollution through intense sulfide oxidation processes in large waste dumps, underground galleries, and open pits, affecting a total surface area of 4,13 km^2 (Moreno-González et al., 2020). However, despite the great variety of mining components, the main pollutant contribution comes from the leaching of existing sulfide waste dumps, exposed to weathering without adopting remediation measures. The different AMD sources are diverted into two different basins (Fig. 1); the Meca River to the south, which feeds the Sancho Reservoir, and the Oraque River to the east, where the Alcolea

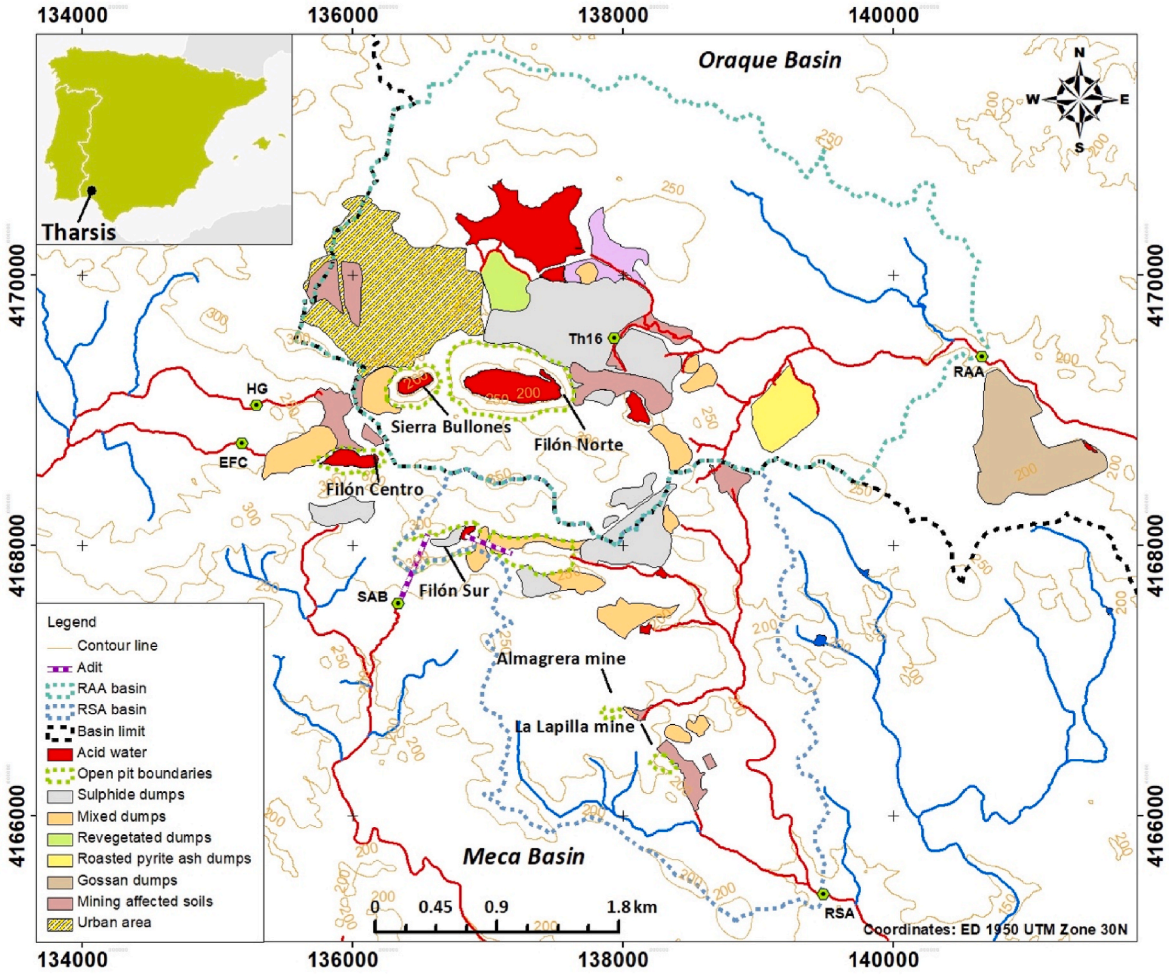

Fig. 1. Location map of the study area showing sampling points, main basins (Oraque and Meca) and sub-basins (RAA and RSA), streams, open pits, and dumps (acidic water is shown in red). (For interpretation of the references to color in this figure legend, the reader is referred to the Web version of this article.)

Reservoir is being built.

The Tharsis area has a Mediterranean climate, characterized by an average temperature of 16.5 °C, with minimum temperatures below 0 °C and maximum temperatures close to 40 °C. Rainfall shows a high intra- and inter-annual variability with an average yearly precipitation close to 600 mm (Galván et al., 2009). The study area is underlain by IPB materials that expand from the Atlantic coast in Portugal to the western part of Spain. The IPB is formed by three lithologic units: the Phyllite-Quartzite Group (PQ), the Volcano-Sedimentary Complex (VSC), and the Culm Group (CG). Numerous sulfide deposits are found in the VSC, which incorporate a mafic-felsic volcanic sequence interstratified with shales. The Tharsis area is constituted by four major south-dipping tectonic units: 1) shales and sandstones of the PQ Group, 2) massive sulfides and slates, 3) slates intruded by basalts with bodies of hydrothermal breccias, and 4) rhyodacite sills intruding shales. The original reserve of sulfide deposits is around 133 Mt and consists mainly of pyrite (more than 90%) and other sulfides such as chalcopyrite, sphalerite, galena, chalcocite, and covellite (Tornos et al., 2009).

3. Methodology

To study the temporal hydrochemical variations of AMD from the Tharsis mines, six different representative sampling points were selected – four AMD sources and two streams receiving leachates from several point and diffuse AMD sources (Fig. 1 and Table SM1): 1) SAB, a leachate flowing out a derelict mine adit, known as La Sabina, built for the drainage and mineral transportation in the mid-19th century (Checkland, 1967). However, this infrastructure was unsuccessful as it was below the mass of sulfide; 2) Th16, a leachate generated from a huge sulfide dump (0.63 km^2) from materials extracted in Filón Norte open pit, exploited until 1999 (Moreno-González et al., 2018). The waste began to be accumulated in 1977–78 according to available aerial orthophotographs, reaching its current shape in 2001; 3) EFC, a leachate generated in a dump (0.12 km^2) mainly consisting of spoil and low sulfidic wastes from the Filón Centro open pit, exploited until 1960; 4) HG, a leachate generated from an area with soils degraded by mining (0.07 km^2) prior to 1977, as evidenced by aerial orthophotographs; 5) RAA, a small stream (basin area of 11.7 km^2) that collects point and diffuse AMD sources flowing to the Oraque River, among them Th16 (Fig. 1); 6) RSA, another small stream (basin area of 6.4 km^2) that collects most leachates flowing to the Meca River, generated from several waste dumps as well as other diffuse sources. These dumps were formed simultaneously with those of Filón Norte (from 1977 to 2001), according to the aerial orthophotographs.

Sampling was undertaken from December 2016 to December 2018, except in the case of Th16 which started in February 2017. The sampling was performed on a fortnightly and monthly frequency during the rainy and dry seasons, respectively. In total, 41 different samplings were performed in each site, however, some of them dried up during the dry season (e.g., HG, n = 23). Samples were filtered through 0.45 μm filters, acidified to pH < 2 with ultrapure HNO_3 and stored in high-density polyethylene bottles that were previously washed with a solution of 10% HNO_3. Collected samples with pH values < 2 were also acidified to follow the same analytical procedure. The flow rate (Q) at each sampling point was estimated by determining the channel section and the water velocity with a flowmeter (FP111 Global Flow Probe). The bucket method was employed in the case of irregular channels and low discharge. Measurements of different physicochemical parameters such as pH, electrical conductivity (EC), oxidation-reduction potential (ORP), and temperature were made in situ at each sampling point with a Crison MM40+ multimeter, which had previously been calibrated with certified solutions. Measured ORP values were referenced to the standard hydrogen electrode (Eh) according to Nordstrom and Wilde (1998).

The samples were analyzed at the R + D laboratories at the University of Huelva: 1) major cations by Inductively Coupled Plasma-Atomic Emission Spectroscopy (ICP-AES); and 2) trace elements by Inductively Coupled Plasma-Mass Spectroscopy (ICP-MS). Detection limits were: 1 mg/L for K; 0.5 mg/L for S; 0.1 mg/L for Al, Ca, Zn; 0.05 mg/L Cu, Fe, Mg; 20 μg/L for As, Cr, Mn, Pb, Sb, Si, V; 0.01 μg/L for Co, Cd, Li, Ni. NIST 1640 certified reference material was used to verify the quality of the analyses, which were performed in triplicate to evaluate the analytical precision (better than 5% in every case). Homemade standards (from certified materials) and blanks were also used to check the accuracy of each analysis sequence. Blank concentrations were below the detection limit of the equipment for most elements.

The PHREEQC code v3.4 (Parkhurst and Appelo, 2013) was used to obtain the chemical speciation and saturation indices of samples, using the Wateq4f database enlarged with thermodynamic data for schwertmannite from Bigham et al. (1996). To assess the metal transport through the different AMD sources during the sampling period, the pollutant load was calculated by multiplying the flow rate by the concentration of each element. Thus, the instantaneous load was determined for each sampling, while the total load was calculated based on the average values. A statistical analysis was performed using the XLSTAT software (Addinsoft®). The correlation among variables was determined according to the Spearman correlation coefficient due to the non-normal distribution followed by most variables studied (Davis, 2002).

4. Results and discussion

4.1. Hydrochemical characteristics of sampling points

The distributions of the flow and physicochemical parameters of the samples are shown in Fig. 2 as box and whiskers plots. As expected, stream samples (RAA and RSA) exhibited the highest flows of the dataset as well as the greatest variability (interquartile range -IR-of 3–13 L/s and 2–14 L/s, respectively; Tables SM2 and SM3). On the other hand, leachates from the La Sabina (SAB) adit had the lowest flow variability (IR of 0.5–1.5 L/s; Table SM4). Values of pH remained below 3 in all samples irrespective of the hydrological conditions observed, with a low variability observed in each sampling point (e.g., IR of 2.4–2.5 in RAA or 2.4–2.6 in EFC and HG; Tables SM2-SM7). The high intensity of sulfide oxidation processes led to high EC values. The highest EC mean was observed in Th16 (23 mS/cm) followed by RAA and RSA (close to 19 mS/cm), exhibiting however in both cases a high variability between samplings (IR of 15–24 and 12–27 in RAA and RSA, respectively; Tables SM2-SM3). On the contrary, HG, SAB, and EFC showed lower EC values (mean values of 3.2 mS/cm, 5.4 mS/cm and 7.6 mS/cm, respectively) and variability than the other points (Fig. 2). This fact is related to the dilution effect caused by runoff after rainfall events, where the studied streams (RAA and RSA) have a larger drainage basin than the AMD sources, hence leading to higher runoff generation. A similar dilution effect related to rainfalls was observed by Masbou et al. (2020) during a 24 h Cu isotopic study in the Meca River. Regarding Eh, HG, and EFC showed the highest oxidation conditions (mean value of 727 mV and 707 mV, respectively), while Th16 showed the lowest ones (mean of 572 mV).

Concerning metal concentrations, HG was the sampling point with the lowest concentration of most pollutants (e.g., median values of 53 mg/L of Al, 2.7 mg/L of Cu, 17 mg/L of Zn, or 1910 mg/L of sulfate; Table SM6), except for Mn, Ni, Pb and Zn which was recorded in SAB (Figs. 3 and 4 and Table SM4). On the contrary, the highest concentrations for most metal/loids were found in RAA, RSA, and Th16 (median values between 1.2 and 1.4 g/L of Al, 3.6, and 4.4 mg/L of Fe, and 25.2 and 31.1 g/L of SO_4, Figs. 3 and 4 and Tables SM2, SM3 and SM7). Pb was found at lower concentrations in the samples, with median values from 24 to 73 μg/L.

The highest Pb contents were found in the stream waters (maximum values of 910 and 831 μg/L in RAA and RSA, respectively). These sampling points also showed the highest concentrations of As and V, with median values of 10,800 and 484 μg/L in RSA and 6101 and 453

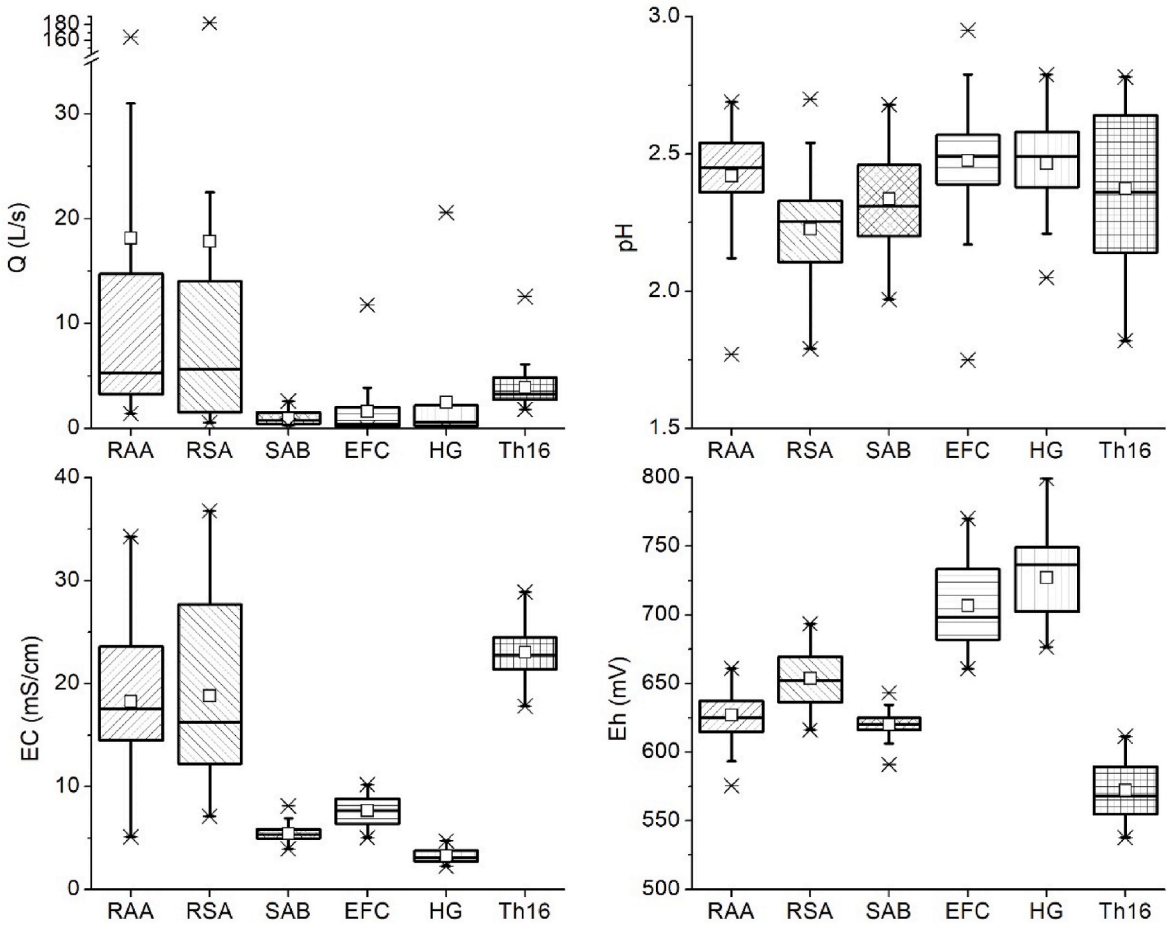

Fig. 2. Box and whiskers plots of flow and physicochemical parameters (n = 41 for RAA, EFC and SAB, n = 40 for RSA, n = 39 for Th16 and n = 23 for HG). The height of each box represents the interquartile range (IR) containing 50% of values, the horizontal line inside the box shows the median value, and the white square indicates the mean value. The whiskers are lines that extend from the box to the highest and lowest values excluding outliers (*). Outliers represent those values being 1.5 larger than the length of the box from its upper or lower border.

μg/L in RAA, respectively (Tables SM2-SM3). On the contrary, the lowest concentrations of As and V were obtained in EFC and HG sampling points (median values < 40 μg/L). The lowest values for other trace metals such as Cd, Co, Cr, and Ni were also observed in HG (Fig. 4). On the other hand, these values are strikingly high if compared with the regional background. For example, Sarmiento et al. (2009a) reported average metal concentrations (e.g., Al, Fe, Cu, Mn or Zn) below 200 μg/L in uncontaminated near-neutral streams (mean pH of 7.2) of the IPB.

4.2. Temporal evolution

Hydrology may be a key parameter controlling metal fluxes from mine sites to the surrounding water bodies, especially in semiarid areas where short but intense rainfall episodes lead to drastic hydrochemical changes (e.g., Anawar, 2013; Cánovas et al., 2017). In this sense, the content of dissolved solids measured by EC is a good indicator of such changes (Fig. SM1). Heavy rains during the sampling period occurred in February 2017 (94 mm), March/April 2018 (282 mm), and November 2018 (161 mm). These rainfall events caused the generation of high flows, with maximum values close to 200 L/s in streams (Tables SM2-SM3). Less important flows were generated during these rainy periods in AMD sources, with values generally below 20 L/s (Tables SM4-SM7). These higher flows coincided with a general decrease in EC values due to dilution with runoff, especially evident in streams (RSA and RAA), while it was not so significant in AMD sources with a more complex hydrogeological behavior. This can be clearly seen in Fig. 6A where the relationship between flow and EC is observed. Whereas stream flows exhibited an inverse correlation with EC values (r = 0.82), no correlation was observed in the AMD sources.

Once the rainfalls ceased, a general increase in EC was observed during summer and the beginning of autumn, especially in stream waters due to the absence of dilution with runoff water and through evaporation along the watercourses. This evolution agrees well with that reported by Sáinz et al. (2002), who studied the leachates generated from mining waste rock dumps of the IPB. These authors reported an initial rapid and intense leaching of the waste dumps, followed by a period of variable duration during which leaching intensity decelerates. In addition, the lack of rainfall events caused the residence time of waters inside the waste rocks to be higher, intensifying the processes of water-rock interactions (Cánovas et al., 2007). As stated before, SAB and Th16 maintained a more constant flow throughout the year and the increases with rainfalls were more smoothed. On the contrary, HG dried out during a long period in summer, while EFC and RSA also only dried occasionally. The temporal evolution of element concentrations is shown in Fig. 5. The concentration of most elements followed the same tendency as those of the EC values (Fig. SM1), with higher values being observed during the dry season, reaching their yearly maximum peaks, and minimum values during the rainy periods (Fig. SM1 and Tables SM2-SM7). However, a different behavior was observed in some AMD sources. For instance, leachates from La Sabina (SAB) showed a delayed response to the rainfall episodes, reaching their maximum and minimum values at a later time. This may be related to the different

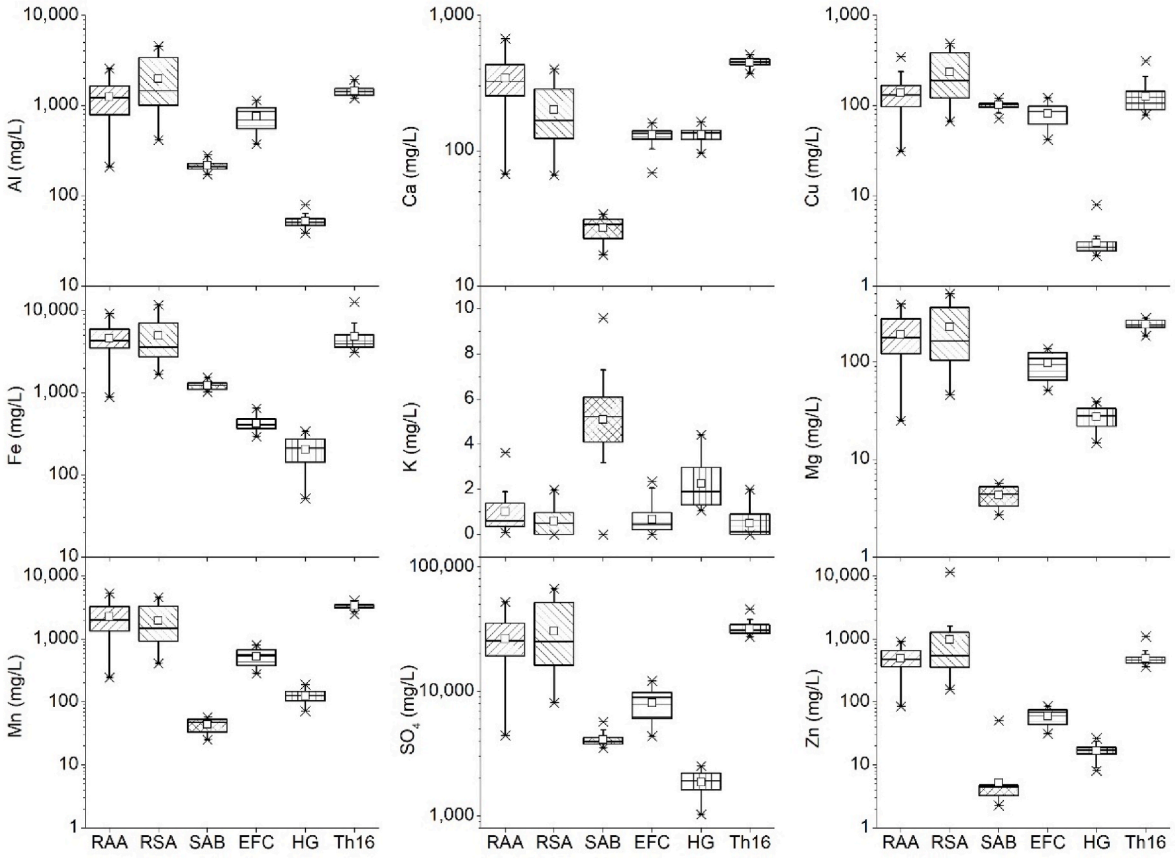

Fig. 3. Box and whiskers plots of the concentration of sulfate and major elements (>1 mg/L) in sampling points (n = 41 for RAA and EFC, n = 40 for RSA and SAB, n = 38 for Th16 and n = 23 for HG).

travel time of water in surface and underground AMD sources, thus, surface AMD sources such as tailings and waste dumps show a quicker response to geochemical processes (e.g., dilution by runoff or redissolution of secondary minerals) than underground AMD sources. On the other hand, concentrations in effluents from Th16 increased notably during the rainy season (maximum values of 1.9 g/L of Al, 12.9 g/L of Fe and 45.8 g/L of SO_4).

Fig. 6B and C shows how the concentrations of sulfate and most elements correlated positively with the flow in this AMD source and, to a lesser extent, in the SAB. This correlation may be related to the washing of Fe-rich evaporitic sulfate salts within the large pyrite-rich spoil heaps. On the contrary, a general inverse relationship was observed between flow and most elements in the rest of the sampling points (Fig. 6B and C). This pattern seems to be related to the different hydrogeological characteristics of the sampling points. In streams, the most important effect is dilution by runoff. On the contrary, in SAB and specially Th16 concentration evolution is smoother due to a longer residence time (also seen through the lower Eh values) and the effect of the washing of sulfide oxidation products. EFC and HG have intermediate conditions due to the smaller size of dumps and mining residues they come from. However, a different remarkable relation was observed for Pb, which exhibits a high positive correlation in all sampling points (r between 0.47 and 0.81), increasing in concentration with rising flows, except for EFC which showed a non-significant correlation.

4.3. Elemental ratios and hydrogeochemical processes

Elemental ratios may provide useful information about the geochemical processes governing the solubility of elements in mine waters. Sulfate can be used as an indicator of geochemical processes due to its quasi-conservative behavior in acidic mine waters (Berger et al., 2000). For example, a Fe/SO_4 mass ratio of 0.29 would represent the dissolution of pyrite, the predominant sulfide exposed to weathering. Thus, values lower than 0.29 would be indicative of Fe precipitation while values above it would indicate the preferential dissolution of Fe oxides (Romero et al., 2006; Cánovas et al., 2016b). The highest ratios of Fe/SO_4 were observed at the SAB sampling point with values close to the theoretical value of pyrite oxidation (Fig. 7), which indicates a low Fe precipitation rate. On the other hand, the lowest Fe/SO_4 ratios occurred in HG and EFC, where the intense precipitation of Fe as secondary minerals may take place (Plumlee et al., 1999; Casiot et al., 2003). The precipitation of secondary Fe minerals has turned out to be a critical factor controlling the solubility of trace metals in AMD sites. In this sense, the availability of Fe(III) is the common limiting factor for Fe mineral precipitation. Once the sulfide is oxidized, Fe(II) is released from the AMD source, which is subsequently oxidized to Fe(III) in the presence of oxygen, giving the water a reddish color. In the study area, SAB and Th16 were the sampling points with the highest percentage of Fe(II) (median value > 95% of Fe_{Total}; Fig. SM2). The waters had a greenish or transparent color at these points (Table SM1). On the contrary, the lowest Fe(II) percentages were observed in EFC and HG, which could be related to the lower volume of wastes they came from, which facilitates the oxygen supply. Stream waters (RAA and RSA) had median values of Fe(II), 90 and 76%, respectively (Fig. SM2), which may probably be due to the strong influence of the ferrous waters from the AMD sources joining these streams, such as those of Th16.

The saturation indices for some minerals that commonly precipitate in AMD-affected waters are shown in Figure SM3. The waters showed supersaturation with respect to jarosite minerals and goethite (median values of SI > 1.4), although in this latter case this mineral may not have precipitated directly from the waters, but following mineral transformation processes (Bigham et al., 1996). The precipitation of these

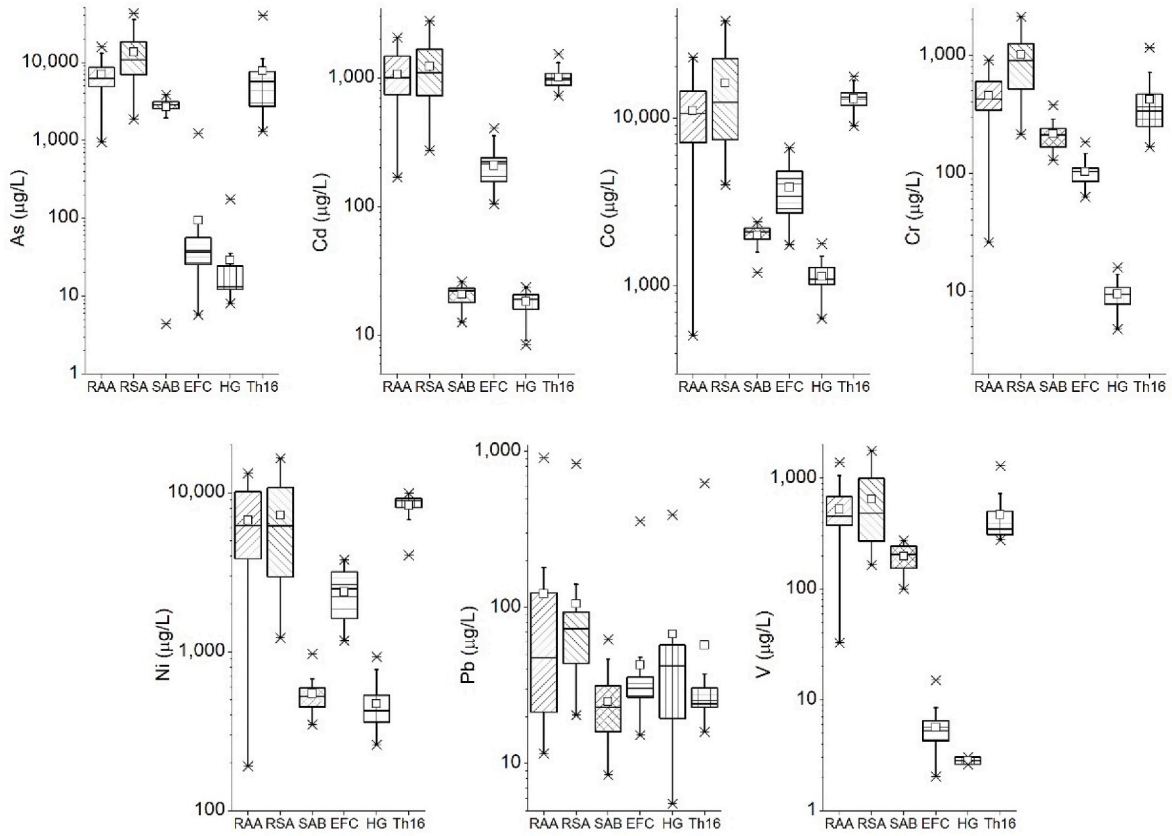

Fig. 4. Box and whiskers plots of the concentration of some trace elements in the sampling points (n = 40 for RAA and EFC, n = 39 for RSA and SAB, n = 37 for Th16 and n = 23 for HG. Some values for As, Pb, V and Cr were below the detection limit; see Tables SM2-SM7).

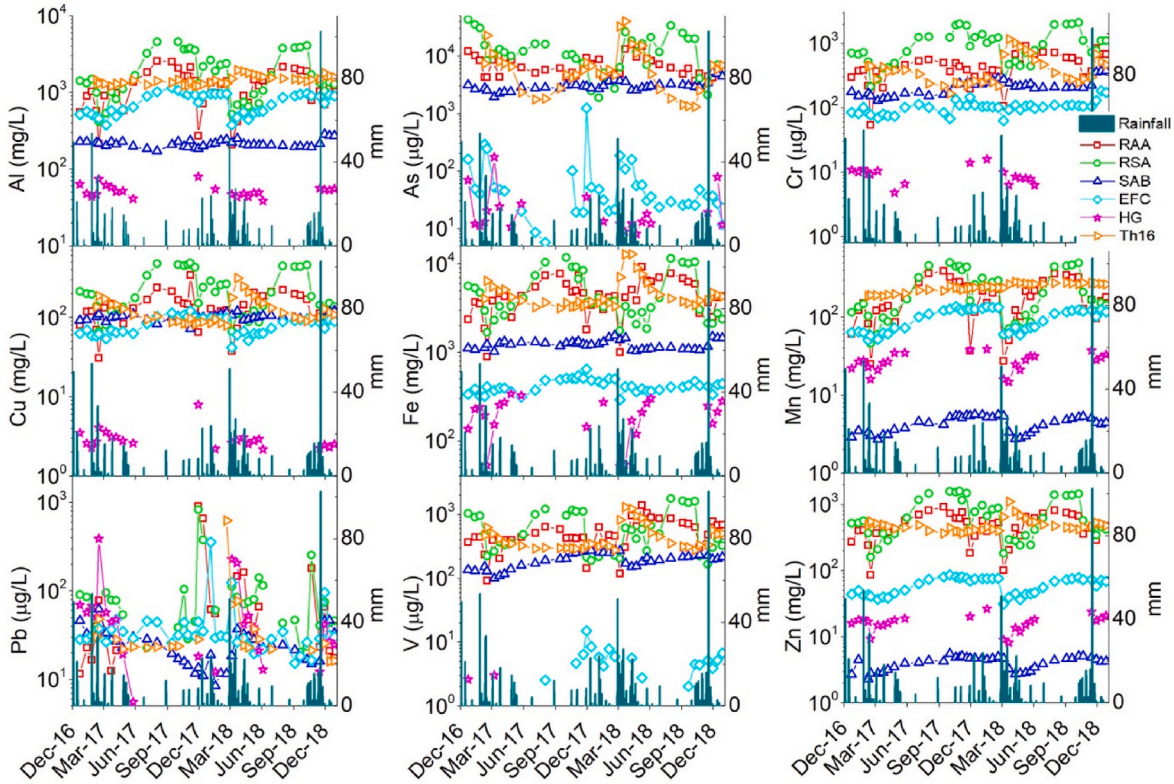

Fig. 5. Temporal evolution of daily rainfall and element concentrations in sampling points.

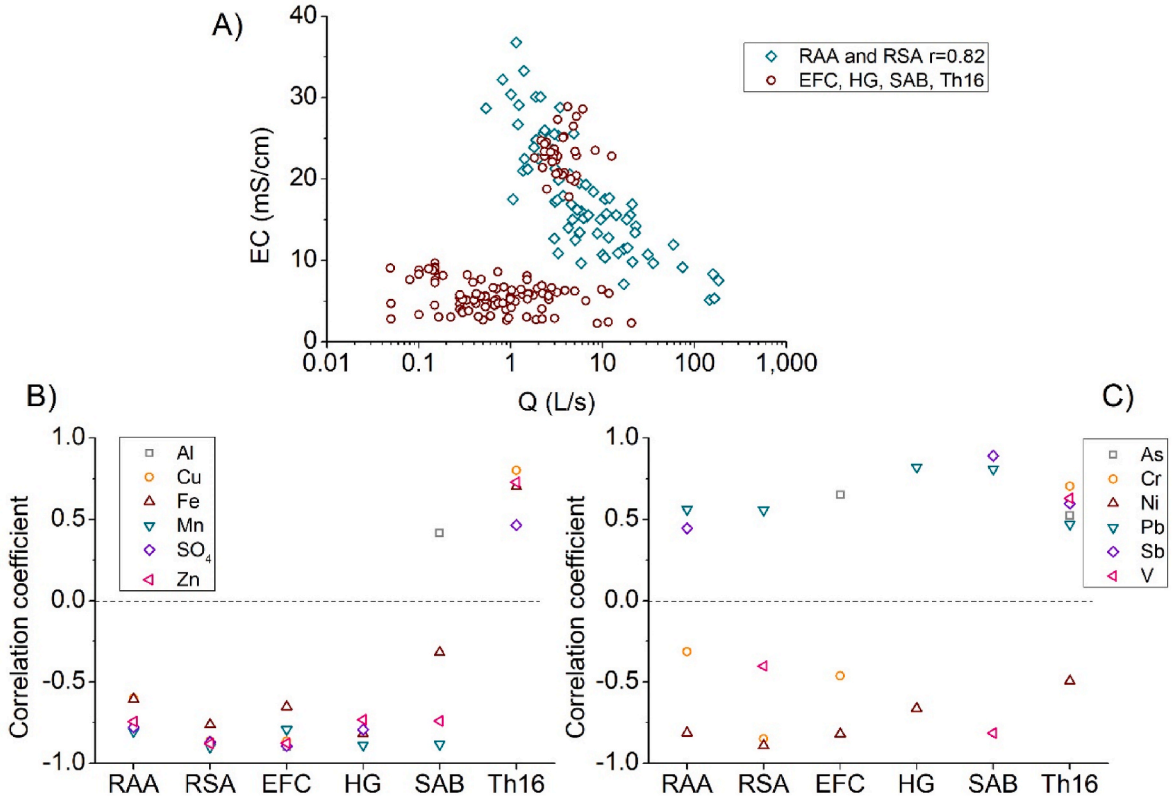

Fig. 6. A) Correlation between flow and EC in both streams (RAA and RSA; blue diamonds) and AMD sources (SAB, EFC, HG and Th16; red circles); B) Spearman correlation coefficient between flow and some major and C) trace elements (only significant values at $p < 0.05$ are shown). (For interpretation of the references to color in this figure legend, the reader is referred to the Web version of this article.)

minerals has been previously reported by other authors in the study area (Caraballo et al., 2011; Valente et al., 2013; Masbou et al., 2020). For example, Valente et al. (2013) identified two different paragenesis, the first one arising from mineral–water interactions involving the primary minerals close to the AMD sources, while the second one, observed downstream of the AMD sources, represents a more evolved paragenesis. Thus, during the first paragenesis, close to AMD sources, Fe sulfates (e.g., szomolnokite, copiapite, coquimbite) and jarosite dominate the efflorescent salts and ochre mineral assemblages, respectively. However, other metal sulfates (e.g., hexahydrite, gypsum, alunogen) and other Fe oxides (e.g., goethite) gain importance in the mineral assemblage downstream the AMD sources. The precipitation of jarositic minerals may scavenge some elements such as K, As, or Tl (Cánovas et al., 2021). For example, the highest K concentrations were observed in SAB (median value of 5.2 mg/L; Fig. 3) due to the higher proportion of Fe(II) that causes a lower precipitation of K-jarosite (median saturation index value of 5.8). Although jarositic mineral precipitation may predominate in the study area, the precipitation of schwertmannite (median values of SI > 1.3; Fig. SM3) may also take place, especially during the rainy period, when sulfate and metal concentrations are generally lower and pH values are slightly higher. On the other hand, waters were undersaturated with respect to copiapite and melanterite, the most common Fe sulfate evaporitic salts in AMD environments. However, these mineral phases were visually observed during the study period and were reported by other authors in the study area (e.g., Valente et al., 2013; Masbou et al., 2020), thus these discrepancies may be related to some uncertainties in the solubility products of these minerals (Basallote et al., 2019).

Sulfate showed a great dispersion and low correlation with As and Pb ($r \leq 0.50$; Fig. 7) in the sampling points due to the intense coprecipitation/sorption processes of these elements onto secondary minerals (Acero et al., 2006; Cánovas et al., 2016b). However, some differences can be observed between the sampling points. For example, SAB showed the highest As/SO_4 ratios due to the low Fe precipitation commented above. Also, RSA, RAA and Th16 displayed high values both of Fe/SO_4 and As/SO_4. On the contrary, HG and EFC showed the lowest As/SO_4 ratios, coinciding with the lowest Fe/SO_4 ratios, indicative of intense Fe precipitation. A similar behavior was also observed for V, indicating that this element may be, like As, sorbed/coprecipitated on Fe secondary minerals (Blackmore et al., 1996). It stands out that in Th16 the sulfate concentrations barely vary, while those of As show a high variability, which suggests that the solubility of As may be related to certain geochemical control rather than to the intensity of sulfide oxidation. It is also remarkable the high negative correlation values observed between sulfate and Pb at HG ($r = -0.82$; Fig. 7), where the highest concentrations of Pb were reached coinciding with the lowest concentrations of sulfate. This seems to indicate a geochemical control of Pb solubility in AMD sources by some sulfate mineral. In this sense, waters were undersaturated in anglesite (Fig. SM3), as previously observed in this area (Moreno-González et al., 2020) and other mining sites of the IPB and worldwide (Nieto et al., 2003; Acero et al., 2006; Nordstrom, 2011; Cánovas et al., 2016b). Some authors (Sarmiento et al., 2009b; Davila et al., 2021) link this increase in Pb concentration to the release through desorption or transformation processes of Fe oxyhydroxysulfates.

Ratios of Co/SO_4 and Ni/SO_4 in all samples are aligned to lines with slopes of 0.0004 and 0.0002, respectively (Fig. 7), indicating that both elements seem to have a similar mineralogical origin and geochemical behavior. Some differences were, however, observed for Zn between sampling points. The highest Zn/SO_4 ratios were found in RAA, RSA and Th16 that collect leachates from recent wastes (mean value of 0.02; Fig. 7). On the other hand, the ratio was lower in SAB, a gallery constructed more than 100 years ago (mean ratio of 0.015), while intermediate ratios were observed in HG and EFC Fig. 7), the origin of which can be traced back between the older and more recent AMD sources. In

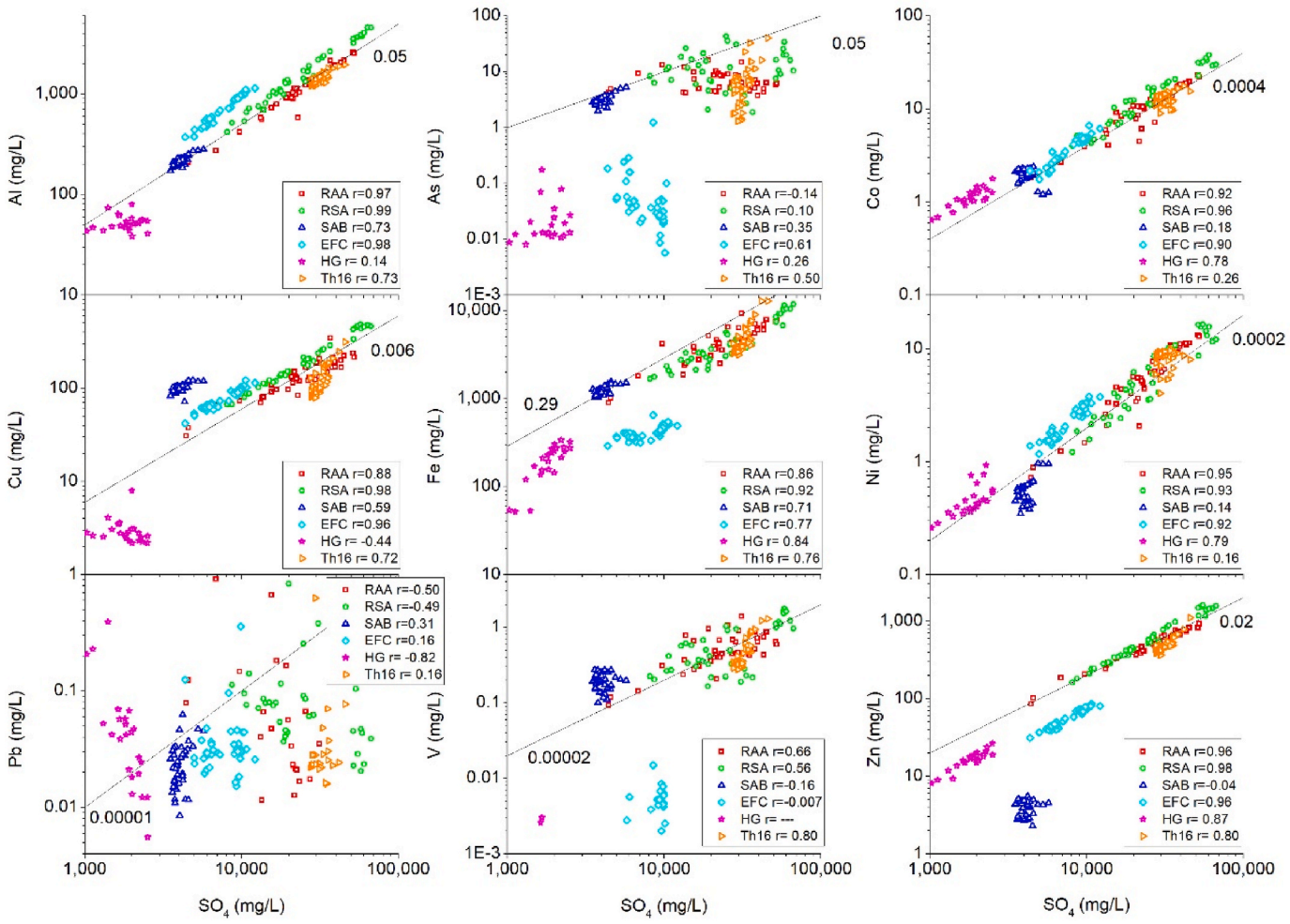

Fig. 7. Relationship between sulfates and several elements in the sampling points. The lines show the representative slope values. The Spearman correlation coefficient for each sampling point is also indicated.

addition to the Zn grade in each mineral deposit, it seems to exist an age-related factor in Zn fluxes from mine wastes due to the decreasing rate of sphalerite weathering with time. This fact has been previously discussed by Vriens et al. (2019) that observed a 30% reduction in Zn concentration in leachates from waste dumps at the Antamina mine (Perú) after ten years of weathering.

4.4. Environmental implications

Metal loadings from mine sites must be quantified to guide the formulation of remediation measures. To address this issue, different approaches can be followed. For example, in mine sites with predominance of waste rock dumps as AMD sources, the metal loadings can be estimated from the precipitation/evapotranspiration values of the study area, the surface of each individual waste dump and the average chemical composition of each AMD. However, the study area is characterized by the existence of diffuse and point sources. For this reason, measuring the flow at each outlet (RSA, RAA, EFC, HG and SAB) and considering the hydrochemical variations of leachates upon different hydrologic conditions, we could calculate realistic figures of pollutant loads delivered by this mine. Figure SM4 shows the temporal evolution of pollutant loads delivered from the Tharsis mine. As expected, the maximum load values were observed in streams (RAA and RSA), which collected main AMD inputs, with maximum values of 27 ton/day of Fe, 7.1 ton/day of Al, 2.5 ton/day of Zn, and so on (Fig. SM4). During the dry periods, the pollutant loads decreased notably down to values close to 1 ton/day of Fe, 0.3 ton/day of Al, and so on. It is remarkable that the average contribution of Th16 to RAA pollutant loading was higher than 76% for Al, Co, Mn, Ni, and SO_4 while the percentage dropped down to 53–64% for trace metal/loids such as As, Cd, Cr, Cu, Fe, V, and Zn. In contrast, the Pb load from Th16 was limited to less than 20% of the total, highlighting the influence of diffuse sources on Pb fluxes. It is to say, except for Pb, that more than 50% of the pollutants reaching the Oraque River from the Tharsis mining zone come from the dumps of Th16.

Table 1 shows the annual pollutant load transported by the Meca and the Oraque rivers during the study period and compares these figures with those obtained in previous works. The pollutant load delivered by the Tharsis mines to the Meca River accounts for 423 ton/yr of Al, 1330 ton/yr of Fe, 47 ton/yr of Mn, and so on. These values are similar to those of previous studies except in the case of the Fe values reported by Cánovas et al. (2016a) because the samples considered in this study were collected in the lower reach of the Meca River, so intense Fe precipitation could take place from the AMD sources. This pollutant load transported by the Meca River reaches the Sancho reservoir (58 hm^3), which has caused the progressive degradation of this reservoir (Cánovas et al., 2016a). In the same way, the Tharsis mines deliver a huge pollutant load to the Oraque River (i.e., 310 ton/yr of Al, 1427 ton/yr of Fe, or 43 ton/yr of Mn). The need for waters to satisfy the growing development of agricultural activities in this area has led to the current construction of a new large reservoir (Alcolea Reservoir, 246 hm^3) at the confluence of the Odiel and Oraque rivers. The Oraque River receives a high load of pollutants not only from the Tharsis mines but also from

Table 1
Pollutant load transported by the Meca and Oraque rivers from Cánovas et al. (2016a), Galván et al. (2009) and mean, minimum, and maximum pollutant loads calculated from AMD waters in this study (in ton/yr).

	Al	Fe	Mn	Zn	As	Cd	Ni
Meca load (ton/yr)							
Mean value of this study	423 (2–2631)	1330 (12–9958)	47 (0.05–304)	146 (0.1–947)	6 (<0.01–49)	0.3 (<0.01–1.9)	1.4 (<0.01–9.5)
Cánovas et al. (2016a)	595	225	90	181			
Oraque load (ton/yr)							
Mean value of this study	310 (74–1083)	1427 (296–9825)	43 (12–143)	134 (34–531)	4.0 (0.3–31)	0.3 (0.06–1)	1.4 (0.5–4.6)
Galván et al. (2009)	418		81	121		0.2	2

other mines located in the Odiel River basin, which may deteriorate the water quality in this reservoir (Olías et al., 2011: Macías et al., 2017). These figures highlight the urgent need for implementing remediation measures in the abandoned mine of Tharsis to fulfil the strict requirements of the WFD to ensure a good quality status of the waters. The recent purchase and exploration of the Tharsis mines by a mining consortium may open doors to significant environmental improvement in this mine site due to the compulsory assumption of the environmental liabilities before starting the exploitation.

5. Conclusions

This study investigated the temporal variations and geochemical processes affecting the hydrochemical composition of the main AMD sources of the Tharsis mines, the second most important mine of the IPB. Values of pH remained below 3 in all waters during the two-year sampling process, irrespective of the hydrological conditions. The intensity of sulfide oxidation processes strongly controlled the hydrochemical composition of the waters, with very high values of EC (median values from 3.1 to 23 mS/cm), sulfate, and metal concentrations.

A high variability was observed in streams due to dilution with runoff, where flow variations were more pronounced, while it was not so significant in AMD sources with more regular and smoother discharges due to the volume of waste dumps (Th16) or its hydrogeological characteristics (SAB). Thus, in Th16, a positive correlation was observed between flow and most metal concentrations while negative values were observed in streams (RAA and RSA). The residence time in sampling points Th16 and SAB was higher and the oxygen supply lower, leading to higher Fe/SO_4, As/SO_4, and V/SO_4 ratios due to the greater proportion of Fe(II) and, consequently, less intense Fe precipitation processes. The lower volume of mining wastes (compared to that of Th16) surrounding EFC and HG may cause intermediate conditions between streams and Th16, characterized by slower groundwater flows.

Lead has a special behavior compared to other elements, since its dissolved concentrations increased during rising flows, probably linked to a mineral solubility control which needs to be further investigated. This fact has significant environmental implications, because Pb pollutant loads increased very abruptly during the wet periods.

Other important factors in metal/oid loadings are the precipitation of secondary minerals, the age of the waste deposits, and the metal grade in wastes. The precipitation of jarositic minerals may limit the mobility of Fe, As, V, and to a lesser extent that of other trace metals, being retained in the waste dumps and streambeds within the mine site. However, this retention does not seem to affect to other trace metals such as Co, Ni, or Mn, which exhibit a more conservative behavior, leading to metal enrichment in the stored waters in the reservoirs. The concentration of Zn in waters seems to be influenced by the original grade in the metal deposit from which the waste was generated together with the age of these wastes. Thus, the older the waste dumps the lower the release of Zn.

The pollutant load delivered by the Tharsis mines to the Meca basin accounts for 423 ton/yr of Al, 1330 ton/yr of Fe, 47 ton/yr of Mn, and minor amounts of other pollutants, while that delivered to the Oraque River sums up to 310 ton/yr of Al, 1427 ton/yr of Fe, or 43 ton/yr of Mn. This pollutant load reaches (or will reach) to freshwater reservoirs, which may cause the progressive contamination of these hydraulic infrastructures, highlighting the urgent need for implementing remediation measures in the abandoned mines of Tharsis.

Credit author statement

R. Moreno-González: Writing - Original Draft, Methodology, Visualization, Writing - Review & Editing, **F. Macías:** Formal Analysis, Validation, Writing - Review & Editing, **M. Olías:** Conceptualization, Funding acquisition, Investigation, Supervision, Writing - Review & Editing, **C.R Cánovas**: Conceptualization, Funding acquisition, Investigation, Supervision, Writing - Review & Editing.

Declaration of competing interest

The authors declare that they have no known competing financial interests or personal relationships that could have appeared to influence the work reported in this paper.

Acknowledgments

This work was supported by the Spanish Ministry of Economic and Competitiveness through the projects CGL2016-78783-C2-1-R (SCYRE) and by H2020 European Institute of Innovation and Technology (EIT RawMaterials) through the projects Modular recovery process services for hydrometallurgy and water treatment (MORECOVERY). C.R Cánovas thanks the Spanish Ministry of Science and Innovation for the Postdoctoral Fellowship granted under application reference RYC2019-027949-I. F. Macias was funded by the R&D FEDER Andalucía 2014–2020 call through the project RENOVAME (FEDER; UHU-1255729). The comments and helpful criticisms of two anonymous reviewers and the support of the Editor have considerably improved the original manuscript and are also gratefully acknowledged. Funding for open access charge: Universidad de Huelva/CBUA

Appendix A. Supplementary data

Supplementary data associated with this article can be found, in the online version, at https://doi.org/10.1016/j.envpol.2021.118697.

References

Acero, P., Ayora, C., Torrento, C., Nieto, J.M., 2006. The behavior of trace elements during schwertmannite precipitation and subsequent transformation into goethite and jarosite. Geochem. Cosmochim. Acta 70, 4130–4139. https://doi.org/10.1016/j.gca.2006.06.1367.

Anawar, H.M., 2013. Impact of climate change on acid mine drainage generation and contaminant transport in water ecosystems of semi-arid and arid mining areas. Phys. Chem. Earth, Parts A/B/C 58, 13–21. https://doi.org/10.1016/j.pce.2013.04.002.

Akcil, A., Koldas, S., 2006. Acid Mine Drainage (AMD): causes, treatment and case studies. J. Clean. Prod. 14, 1139–1145. https://doi.org/10.1016/j.jclepro.2004.09.006.

Basallote, M.D., Canovas, C.R., Olías, M., Pérez-López, R., Macías, F., Carrero, S., Ayora, C., Nieto, J.M., 2019. Mineralogically-induced metal partitioning during the evaporative precipitation of efflorescent sulfate salts from acid mine drainage. Chem. Geol. 530, 119339. https://doi.org/10.1016/j.chemgeo.2019.119339.

Blackmore, D.P.T., Ellis, J., Riley, P.J., 1996. Treatment of a vanadium-containing effluent by adsorption/coprecipitation with iron oxyhydroxide. Water Res. 30, 2512–2516. https://doi.org/10.1016/0043-1354(96)00080-2.

Berger, A.C., Bethke, C.M., Krumhansl, J.L., 2000. A process model of natural attenuation in drainage from a historic mining district. Appl. Geochem. 15, 655–666.
Bigham, J.M., Schwertmann, U., Traina, S.J., Winland, R.L., Wolf, M., 1996. Schwertmannite and the chemical modeling of iron in acid sulfate waters. Geochem. Cosmochim. Acta 60 (12), 2111–2121.
Bird, G., 2016. The influence of the scale of mining activity and mine site remediation on the contamination legacy of historical metal mining activity. Environ. Sci. Pollut. Res. 23, 23456–23466. https://doi.org/10.1007/s11356-016-7400-z.
Cánovas, C.R., Olías, M., Nieto, J.M., Sarmiento, A.M., Cerón, J.C., 2007. Hydrogeochemical characteristics of the Odiel and Tinto rivers (SW Spain). Factors controlling metal contents. Sci. Total Environ. 373, 363–382. https://doi.org/10.1016/j.scitotenv.2006.11.022.
Cánovas, C.R., Olías, M., Macías, F., Torres, E., San Miguel, E.G., Galván, L., Ayora, C., Nieto, J.M., 2016a. Water acidification trends in a reservoir of the iberian pyrite belt (SW Spain). Sci. Total Environ. 541, 400–411. https://doi.org/10.1016/j.scitotenv.2015.09.070.
Cánovas, C.R., Macías, F., Pérez-López, R., 2016b. Metal and acidity fluxes controlled by precipitation/dissolution cycles of sulfate salts in an anthropogenic mine aquifer. J. Contam. Hydrol. 188, 29–43. https://doi.org/10.1016/j.jconhyd.2016.02.005.
Cánovas, C.R., Macías, F., Olías, M., Pérez López, R., Nieto, J.M., 2017. Metal-fluxes characterization at a catchment scale: study of mixing processes and end-member analysis in the Meca River watershed (SW Spain). J. Hydrol. 550, 590–602. https://doi.org/10.1016/j.jhydrol.2017.05.037.
Cánovas, C.R., Macías, F., Olías, M., 2018. Hydrogeochemical behavior of an anthropogenic mine aquifer: implications for potential remediation measures. Sci. Total Environ. 636, 85–93. https://doi.org/10.1016/j.scitotenv.2018.04.270.
Cánovas, C.R., Macías, F., Basallote, M.D., Olías, M., Nieto, J.M., Pérez-López, R., 2021. Metal(loid) release from sulfide-rich wastes to the environment: the case of the Iberian Pyrite Belt (SW Spain). Current Opinion in Environmental Science & Health 20, 100240. https://doi.org/10.1016/j.coesh.2021.100240.
Caraballo, M.A., Sarmiento, A.M., Sanchez-Rodas, D., Nieto, J.M., Parviainen, A., 2011. Sea-sonal variations in the formation of Al and Si rich Fe-stromatolites, in the highly pol-luted acid mine drainage of Agua Agria Creek (Tharsis, SW Spain). Chem. Geol. 284, 97–104. https://doi.org/10.1016/j.chemgeo.2011.02.012.
Casiot, C., Morin, G., Juillot, F., Bruneel, O., Personné, J.C., Leblanc, M., Duquesne, K., Bonnefoy, V., Elbaz-Poulichet, F., 2003. Bacterial immobilization and oxidation of arsenic in acid mine drainage (Carnoulés creek France). Water Res. 37, 2929–2936. https://doi.org/10.1016/S0043-1354(03)00080-0.
Checkland, S.G., 1967. The Mines of Tharsis. Roman, French and British Entreprise in Spain. George Allen & Unwin Ltd, London, p. 288.
Davis, J.C., 2002. Statistics and Data Analysis in Geology. John Wiley & Sons, USA.
Davila, J.M., Sarmiento, A.M., Aroba, J., Fortes, J.C., Grande, J.A., Santisteban, M., Cordoba, F., Leiva, M., Luís, A.T., 2021. Application of a fuzzy logic based methodology to validate the hydrochemical characterization and determining seasonal influence of a watershed affected by acid mine drainage. Nt. J. Environ. Res. Public Health 18 (9), 4693. https://doi.org/10.3390/ijerph18094693, 2021.
EU Commission, 2000. Directive 2000/60/EC of the European Parliament and of the Council, of 23 October 2000, establishing a framework for Community action in the field of water policy. Off. J. Eur. Econ. L 327 (1), 22.12.2000 https://eur-lex.europa.eu/legal-content/EN/TXT/?uri¼CELEX:32000L0060.
Galván, L., Olías, M., Fernández de Villarán, R., Domingo Santos, J.M., Nieto, J.M., Sarmiento, A.M., Cánovas, C.R., 2009. Application of the SWAT model to an AMD affected river (Meca River, SW Spain). Estimation of transported pollutant load. J. Hydrol. 377, 445–454. https://doi.org/10.1016/j.jhydrol.2009.09.002.
Grande, J., Valente, T., De la Torre, M.L., Santisteban, M., Cerón, J., Pérez-Ostalé, E., 2014. Characterization of acid mine drainage sources in the Iberian Pyrite Belt: base methodology for quantifying affected areas and for environmental management. Environ. Earth Sci. 71, 2729–2738. https://doi.org/10.1007/s12665-013-2652-0, 2014.
Gonzalo y Tarín, J., 1888. Descripción física, geológica y minera de la provincia de Huelva. Memorias de la Comisión del Mapa Geológico de España, Tomo II, Madrid, p. 660.
Johnson, D.B., Hallberg, K.B., 2005. Acid mine drainage remediation options: a review. Sci. Total Environ. 338, 3–14. https://doi.org/10.1016/j.scitotenv.2004.09.002.
Leistel, J.M., Marcoux, E., Thiéblemont, D., Quesada, C., Sanchez, A., Almodóvar, G.R., Pascual, E., Sáez, R., 1998. The volcanic-hosted massive sulphide deposits of the Iberian Pyrite Belt. Miner. Deposits 33, 2–30.
Macías, F., Pérez-López, R., Caraballo, M.A., Sarmiento, A.M., Cánovas, C.R., Nieto, J.M., Olías, M., Ayora, C., 2017. A geochemical approach to the restoration plans for the Odiel River basin (SW Spain), a watershed deeply polluted by acid mine drainage. Environ. Sci. Pollut. Res. 24, 4506–4516. https://doi.org/10.1007/s11356-016-8169-9.
Masbou, J., Viers, J., Grande, J.A. Freydier R., Zouiten, C., Seyler, P., Pokrovsky, O.E., Behra, P., Dubreuil, B., de la Torre, M.L., 2020. Strong temporal and spatial variation of dissolved Cu isotope composition in acid mine drainage under contrasted hydrological conditions. Environ. Pollut. 266, 115104. https://doi.org/10.1016/j.envpol.2020.115104.
Mighanetara, K., Braungardt, C.B., Rieuwerts, J.S., Azizi, F., 2009. Contaminant fluxes from point and diffuse sources from abandoned mines in the River Tamar catchment, UK. J. Geochem. Explor. 100, 116–124.
Moreno-González, R., Olías, M., Macías, F., Cánovas, C.R., de Villarán, R.F., 2018. Hydrological characterization and prediction of flood levels of acidic pit lakes in the Tharsis mines, Iberian Pyrite Belt. J. Hydrol. 566 https://doi.org/10.1016/j.jhydrol.2018.09.046.
Moreno-González, R., Cánovas, C.R., Olías, M., Macías, F., 2020. Seasonal variability of extremely metal rich acid mine drainages from the Tharsis mines (SW Spain). Environ. Pollut. 259 https://doi.org/10.1016/j.envpol.2019.113829.
Nieto, J.M., Capitán, M.A., Sáez, R., Almodóvar, G.R., 2003. Beudantite: a natural sink for as and Pb in sulphide oxidation processes. Trans. Inst. Min. Metall. B 112, 293–296. https://doi.org/10.1179/037174503225003134.
Nordstrom, D.K., Wilde, F.D., 1998. Reduction–oxidation Potential (Electrode Method). National Field Manual for the Collection of Water Quality Data, Book 9, Chapter 6.5. U.S. Geological Survey Techniques of Water-Resources Investigations. U.S. Geological Survey, Reston, VA, p. 20.
Nordstrom, D.K., 2011. Hydrochemical process governing the origin, transport and fate of major and trace elements from mine wastes and mineralized rock to surface waters. Appl. Geochem. 26, 1777–1791. https://doi.org/10.1016/j.apgeochem.2011.06.002.
Nordstrom, D.K., Blowes, D.W., Ptacek, C.J., 2015. Hydrogeochemistry and microbiology of mine drainage: an update. Appl. Geochem. 57, 3–16. https://doi.org/10.1016/j.apgeochem.2015.02.008.
Olías, M., Nieto, J.M., Sarmiento, A.M., Cánovas, C.R., Galván, L., 2011. Water quality in the future Alcolea Reservoir (Odiel River, SW Spain): a clear example of the inappropriate management of water resources in Spain. Water Resour. Manag. 25, 201–215. https://doi.org/10.1007/s11269-010-9695-8.
Parkhurst, D.L., Appelo, C.A.J., 2013. Description of input and examples for PHREEQC version 3—a computer program for speciation, batch-reaction, one-dimensional transport, and inverse geochemical calculations. U.S. Geological Survey Techniques and Methods, book 6, 497. https://doi.org/10.3133/tm6A43 chap. A43.
Pinedo Vara, I., 1963. Piritas de Huelva. Su historia, minería y aprovechamiento. Summa, Madrid.
Plumlee, G.S., Smith, K.S., Montour, M.R., Ficklin, W.H., Mosier, E.L., 1999. Geologic controls on the composition of natural waters and mine waters draining diverse mineral-deposit types. In: Filipek, L.H., Plumlee, G.S. (Eds.), The Environmental Geochemistry of Mineral Deposits. Part B: Case Studies and Research Topics. Society of Economic Geologists, Littleton, 6B. Reviews in Economic Geology, pp. 373–432.
Romero, A., González, I., Galan, E., 2006. The role of efflorescent sulfate salts in the storage of trace elements in stream waters polluted by Acid Mine Drainage: the case of Peña del Hierro, southwestern Spain. Can. Mineral. 44, 1431–1446. https://doi.org/10.2113/gscanmin.44.6.1431.
Sáinz, A., Grande, J.A., de la Torre, M.L., Sánchez-Rodas, D., 2002. Characterisation of se-quential leachate discharges of mining waste rock dumps in the Tinto and Odiel rivers. J. Environ. Manag. 64, 345–353. https://doi.org/10.1006/jema.2001.0497.
Sarmiento, A.M., Nieto, J.M., Olías, M., Cánovas, C.R., 2009a. Hydrochemical characteristics and seasonal influence on the pollution by acid mine drainage in the Odiel river Basin (SW Spain). Appl. Geochem. 24 (4), 697–714. https://doi.org/10.1016/j.apgeochem.2008.12.025.
Sarmiento, A., Nieto, J., Casiot, C., Elbaz-Poulichet, F., Egal, M., 2009b. Inorganic arsenic speciation at River basin scales: the Tinto andOdiel rivers in the iberian pyrite belt, SW Spain. Environ. Pollut. 157, 1202–1209. https://doi.org/10.1016/j.envpol.2008.12.002.
Tornos, F., Gonzalez Clavijo, E., Spiro, B., 1998. The Filon Norte orebody, Tharsis, Iberian Pyrite Belt: a proximal low-temperature shale-hosted massive sulphide in a thin- skinned tectonic belt. Miner. Deposits 33, 150–169.
Tornos, F., 2006. Environment of formation and styles of volcanogenic massive sulfides: the Iberian Pyrite Belt. Ore Geol. Rev. 28, 259–307. https://doi.org/10.1016/j.oregeorev.2004.12.005.
Tornos, F., Lopez-Pamo, E., Sánchez España, F.J., 2009. The Iberian pyrite belt. In: Agueda, J., Palacios, J., Salvador, C.I. (Eds.), Spanish Geological Framework and Geosites. IGME, Madrid, pp. 56–64.
Valente, T., Grande, J., De La Torre, M., Santisteban, M., Cerón, J.C., 2013. Mineralogy and environmental relevance of AMD-precipitates from the Tharsis mines, Iberian pyrite Belt (SW, Spain). Appl. Geochem. 39, 11–25. https://doi.org/10.1016/j.apgeochem.2013.09.014.
Vriens, B., Peterson, H., Laurenzi, L., Smith, L., Aranda, C., Mayer, K.U., Beckie, R.D., 2019. Long-term monitoring of waste-rock weathering at the Antamina mine, Peru. Chemosphere 215, 858–869. https://doi.org/10.1016/j.chemosphere.2018.10.105.